Pressure-Relief Impact Control of Open Circuit Hydraulic Pump-Controlled Forging Press System

Authors:

Xiaoming Cao, Jing Yao, Tong Sha, Yu Song

Abstract:

Taking the open circuit hydraulic pump-controlled forging press system as the research object, according to the problems of pressure-relief impact of this system, the pressure-relief rules, mathematic models of the energy release rules, and the flow release rules were established, and the pressure-relief performance in different stages of each pressure-relief curve was analyzed. Based on the different requirements of the pressure gradient decrease, the combined pressure-relief curve (CPRC) was proposed to realize variable-pump eccentric magnitude planning. An experimental study on the pressure-relief process with CPRC was carried out. The results show that the pressure fluctuation of the pressure-relief pipe was reduced and the suppression effect of pressure-relief impact was better than that of the single regular pressure-relief curve. When the initial pressures were 10 MPa and 15 MPa, the pressure impact of the pressure-relief tube decreased by 45.45% and 37.5%, respectively, which realized the smooth pressure relief of the main cylinder.

Pressure-Relief Impact Control of Open Circuit Hydraulic Pump-Controlled Forging Press System

Xiaoming Cao [1] , Jing Yao [1,2,]*, Tong Sha [1] and Yu Song [1]

[1] School of Mechanical Engineering, Yanshan University, Qinhuangdao 066004, China;
   xiaomingzjk@126.com (X.C.); shala1995@gmail.com (T.S.); s18712773072@126.com (Y.S.)
[2] School of Mechanical Engineering, Nanjing Institute of Technology, Nanjing 211167, China
* Correspondence: jyao@ysu.edu.cn; Tel.: +86-1309-136-8419

Abstract: Taking the open circuit hydraulic pump-controlled forging press system as the research object, according to the problems of pressure-relief impact of this system, the pressure-relief rules, mathematic models of the energy release rules, and the flow release rules were established, and the pressure-relief performance in different stages of each pressure-relief curve was analyzed. Based on the different requirements of the pressure gradient decrease, the combined pressure-relief curve (CPRC) was proposed to realize variable-pump eccentric magnitude planning. An experimental study on the pressure-relief process with CPRC was carried out. The results show that the pressure fluctuation of the pressure-relief pipe was reduced and the suppression effect of pressure-relief impact was better than that of the single regular pressure-relief curve. When the initial pressures were 10 MPa and 15 MPa, the pressure impact of the pressure-relief tube decreased by 45.45% and 37.5%, respectively, which realized the smooth pressure relief of the main cylinder.

Keywords: open circuit hydraulic pump-controlled system; forging press; pressure-relief impact; combined pressure-relief curve (CPRC)

1. Introduction

The forging hydraulic press is a key piece of equipment in heavy machinery and plays a pivotal role in the machinery manufacturing industry. The transmission forms of the forging hydraulic press system are mainly divided into two types: valve-controlled and pump-controlled. Due to the low cost, easy maintenance, and relatively low oil cleanliness requirements of valve-controlled systems, it has become the mainstream form of forging hydraulic presses. However, with the increasing energy crisis, green forging is getting more and more attention, and pump-controlled technology has become a hot research topic because of its enormous advantages in energy saving [1,2].

The pump-controlled system is mostly a closed circuit system, mainly used in engineering machinery such as vibratory rollers, cement mixers, and asphalt pavers [3,4]. Generally, the closed circuit pump-controlled cylinder system can be divided into the Closed Circuit Pump-controlled Symmetrical Cylinder Systems (CCPSCS), such as ship steering system [5], and Closed Circuit Pump-controlled Asymmetric Cylinder Systems (CCPACS). The CCPACS adopts a bidirectional variable mechanism to realize the reversing of the inlet and outlet, avoiding throttling loss and overflow loss, and has the advantages of economy, energy saving, and low installed power [6–8]. Zimmerman, J. [9] applied CCPACS to the forging hydraulic press, and the system had a good dynamic response, good control characteristics, a stable operation, and a fast forging speed. However, the CCPACS has the characteristic of flow imbalance, so a large flow charge pump must be added, and it also has the problems of low power recovery rate and large system fever, etc. [10].

We propose an Open Circuit Pump-controlled Asymmetric Cylinder System (OCPACS) to address the above issues, and we apply it to the forging hydraulic press system. The principle of the Open Circuit Pump-controlled Forging Hydraulic System (OCPFHS) is shown in Figure 1. The OCPFHS uses two pumps to control the two cylinder chambers independently, which solves the two-chamber flow asymmetry problem. At the same time, the large flow-charge pump with low pressure oil supplement is omitted, thus improving the energy utilization efficiency. In previous work, we studied the control characteristics [11], energy consumption characteristics [12], control coupling characteristics [13,14], accumulator fast-forging circuit-control characteristics and their influencing factors [15], and long pipeline characteristics [16] of the OCPFHS.
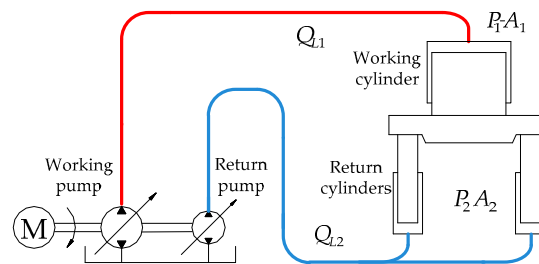

Figure 1. The Open Circuit Pump-controlled Forging Hydraulic System (OCPFHS) diagram.

When the hydraulic press system completes the reduction process, it is necessary to quickly release the high pressure oil in the working cylinder before the return stroke, which is called the pressure-relief process [17,18]. If the pressure-relief process is not handled properly, it will cause impact and vibration of the pipeline and frame. The pressure-relief impact control of hydraulic presses has always been a subject of great concern in academia and the engineering technology field.

Consensus on the formation and development mechanism of pressure relief has not yet been reached. At present, researches mainly focus on the valve-controlled hydraulic press system, including analyzing the transmission rule of the pressure wave in the pipeline [19,20], proposing the active compensation method for the pressure-impact prediction of the directional valve [21,22], using the electro-hydraulic proportional cartridge valve as the pressure-relief valve [23], and designing an energy sinusoidal pressure-relief curve [24]. However, research on the pressure-relief process of pump-controlled hydraulic presses has rarely been reported.

Referring to the design method of the relief curve of the electro-hydraulic proportional cartridge valve to solve these problems, this paper studies the pressure-relief impact control of the OCPFHS, puts forward the combined pressure-relief curve (CPRC), and deduces the mathematical model of CPRC. The simulation and experimental results verify the pressure-relief impact-suppression effect of CPRC, which proves the effectiveness of this pressure-relief method.

2. Pressure-Relief Mechanism

2.1. Energy Storage Characteristics Analysis

After the hydraulic press system completes the working process, the hydraulic system stores a lot of high pressure oil. While the mechanical structure of the main body frame, pipelines, and working cylinder are deformed because of the high pressure, the elastic potential energy is stored. All the energy needs to be released through the oil in the working cylinder and pipelines during the pressure-relief process [25].

2.1.1. Working Cylinder Oil Compression Energy Storage

According to the oil compression equation, the working cylinder oil compression is [26],

$$\Delta V = \frac{\Delta P}{E - P} V_0 \tag{1}$$

where V_0 is the working cylinder oil volume before pressure relief, ΔV is the working cylinder oil compression volume, E is the effective fluid bulk modulus, ΔP is the working cylinder pressure variation, and P is the working cylinder pressure.

Since $P << E$, so $E - P \approx E$, and the working cylinder oil compression is,

$$\Delta V = \frac{\Delta P}{E} V_0. \tag{2}$$

Regardless of the elastic potential energy generated by the expansion of the working cylinder, the working cylinder fluid compression energy is,

$$\Delta W_1 = P \Delta V \tag{3}$$

where ΔW_1 is the working cylinder oil compression energy variation.

According to Equations (2) and (3),

$$\Delta W_1 = \frac{P}{E} V_0 \Delta P. \tag{4}$$

The integral of Equation (4) can be obtained,

$$\int_0^{W_1} \mathrm{d}W_1 = \int_0^P \frac{V_0}{E} P \mathrm{d}P. \tag{5}$$

Therefore, the working cylinder fluid compression energy storage is as follows,

$$W_1 = \frac{1}{2} \frac{V_0}{E} P^2. \tag{6}$$

2.1.2. Frame Elastic-Deformation Energy Storage

The frame diagram of the hydraulic press is shown in Figure 2. Before pressure relief, the hydraulic press frame elastic-deformation energy storage is mainly composed of the deformation energy storage of the upper beam, the moving beam, the columns, and tension-bolt. Since the upper beam and the moving beam all have greater quality and strength, the deformation is very small. However, the deformation of the columns and tension-bolt are larger, and a higher energy is stored.
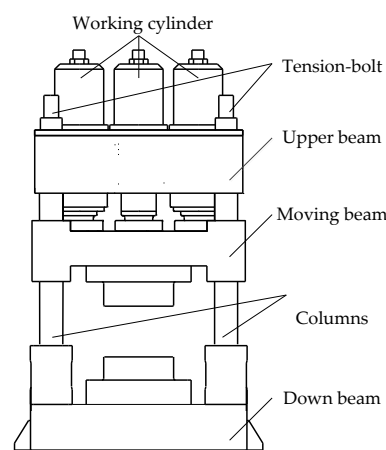

Figure 2. The frame diagram of the hydraulic press.

The deformation of the columns and the tension-bolt is as follows,

$$\lambda_z = \frac{L_z}{E_z A_z} F_z \tag{7}$$

where L_z is the length of the columns and tension-bolt, E_z is the effective fluid bulk modulus of the columns and tension-bolt, A_z is the equivalent cross-sectional area of the columns and tension-bolt, and F_z is the load of a single column and tension-bolt.

The load of a single column and tension-bolt is as follows,

$$F_z = \frac{\pi n_1}{4 n_2} D_1^2 P \tag{8}$$

where D_1 is the inside diameter of the working cylinder, n_1 is the number of working cylinders, and n_2 is the number of columns and tension-bolts.

Energy storage of columns and tension-bolt is,

$$W_2 = n_2 \int_0^{\lambda_z} F_z d\lambda_z. \tag{9}$$

According to Equations (7) and (9),

$$W_2 = n_2 \int_0^{\lambda_z} \frac{E_z A_z}{L_z} \lambda_z d\lambda_z = \frac{1}{2} n_2 \lambda_z F_z. \tag{10}$$

According to Equations (7), (8) and (10),

$$W_2 = \frac{\pi^2 L_z D_1^4 n_1^2}{32 E_z A_z n_2} P^2. \tag{11}$$

Assuming that $\lambda = \pi^2 L_z D_1^4 n_1^2 / 32 E_z A_z n_2$, then the elastic-deformation energy storage of the columns and tension-bolt is,

$$W_2 = \lambda P^2. \tag{12}$$

Therefore, before pressure relief, the total energy storage of the hydraulic press system is mainly the compression energy of the cylinder oil and the elastic-deformation energy of the frame. The total energy storage of the system is as follows,

$$W = W_1 + W_2 = \frac{1}{2} \frac{V_0}{E} P^2 + \lambda P^2. \tag{13}$$

2.2. Energy Storage Characteristics Analysis

2.2.1. Oil Compression Energy Storage Characteristics

Assuming that the amount of oil compression changes from the highest pressure to zero, then the compression energy stored in the working cylinder before the pressure relief is obtained by Equations (2) and (6),

$$W_1 = \frac{1}{2} \frac{\Delta V^2}{V_0} E. \tag{14}$$

The effective fluid bulk modulus of oil is determined by the pressure, temperature, gas content, etc. Since the pressure-relief time is very short, assuming that the temperature and gas content keep invariant, then the rule of effective fluid bulk modulus variation with pressure [27] is,

$$E = 6 \times 10^8 \times \log_{10}\left(\frac{99P}{10^7} + 1\right). \tag{15}$$

It is known from Equations (14) and (15) that when the working cylinder pressure increases, the rule of the oil compression energy storage of the working cylinder is consistent with the rule of the effective fluid bulk modulus variation with pressure, and the energy gradient gradually becomes

smaller. Therefore, with the increase of the working cylinder pressure, the change tendency of the compression energy storage of the working cylinder is initially fast and then slow.

2.2.2. Frame Elastic-Deformation Energy Storage Characteristics

The frame elastic-deformation energy storage is mainly composed of the elastic-deformation energy storage of the column and tension-bolt. According to the Equation (12), with the increase of the working cylinder pressure, the change tendency of the frame elastic-deformation energy storage is initially slow and then fast.

2.2.3. Pressure Energy Storage Characteristics of OCPFHS

Taking the 0.6 MN forging press experimental platform as the research object, the energy storage state of the system before the pressure relief was analyzed. The system parameters under a certain condition are shown in Table 1.

Table 1. Energy storage state parameters of the 0.6 MN forging press test-bed before the pressure relief under a certain condition.

Variable	Name	Value	Unit
L_z	The length of columns and tension-bolt	1.52	m
A_z	The equivalent cross-sectional area of columns and tension-bolt	1.26×10^{-3}	m^2
E_z	The effective fluid bulk modulus of columns and tension-bolt	210	GPa
n_1	The number of the working cylinders	1	-
n_2	The number of columns and tension-bolts	4	-
h_{01}	The initial position of the working cylinder	0.15	m
V_0	The initial oil volume of the working cylinder	3.93×10^{-4}	m^3
P_0	The initial pressure of the working cylinder	250	bar

Taking these condition parameters into Equations (6) and (12), the oil compression energy storage and the frame elastic-deformation energy storage of the 0.6 MN forging press are, respectively, as follows, W_1 = 175.5 J and W_2 = 27.7 J.

That is, the frame elastic-deformation energy storage is about 13.6% of the total energy storage. Therefore, the oil compression energy storage before the pressure relief is the main factor determining the variation of the energy storage.

2.2.4. Pressure-Relief Impact Characteristics

Using the mathematical model deduced in reference [12] and MATLAB/Simulink simulation platform (MATLAB 2010 a, MathWorks, Natick, MA, USA, 2010) to establish the simulation model of OCPFHS, a step signal was used to relieve the pressure of the OCPFHS, and the variable-pump eccentric magnitude curve, working cylinder pressure curve, and relief pipe (connected with the low pressure port of the variable pump, supplied with 8 bar charge pressure in the actual system) pressure curve were obtained under the initial pressure of 100 bar, as shown in Figure 3. In the simulation, the 0–0.1 s was the 100 bar packing stage, and the 0.1–0.5 s was the pressure-relief process. In this paper, the variable-pump eccentric magnitude was characterized by the given voltage variation, and the command voltage of the variable pump was 0–10 V, corresponding to the eccentric magnitude of −5–5 mm.

As shown in Figure 3, when the OCPFHS adopts step pressure relief, the working cylinder pressure decreases rapidly, and realizes pressure relief in a short time. However, the working cylinder pressure fluctuates during the descent process, and the peak pressure in the relief pipe is 10.398 bar, which exceeds the steady pressure of 29.97%, indicating that the pressure-relief process produces a strong pressure-relief impact.

In order to avoid the pressure-relief impact and realize the smooth operation of the OCPFHS, it is necessary to select a reasonable pressure-relief curve according to the energy storage variation rule of the system to realize the pressure-relief impact control.
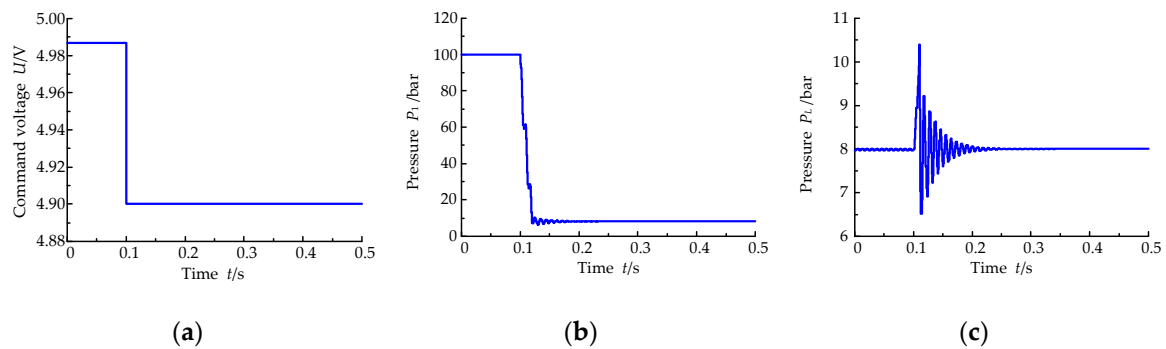
Figure 3. The simulation curve under the step pressure-relief rule. (**a**) Eccentric magnitude; (**b**) Working cylinder pressure; (**c**) Relief-pipe pressure.

3. Pressure-Relief Curve

One of the main influencing factors of the stability and life of forging hydraulic press is the degree of pressure-relief impact, and the quality of its control directly determines the working characteristics and production efficiency of the equipment. The optimal control should be sought by considering the optimal working characteristics and high production efficiency as the control objectives of pressure relief.

3.1. Mathematical Model of the Pressure-Relief Curve

To solve the problem of pressure-relief impact, a reasonable pressure-relief curve should be selected. By analyzing the mathematical characteristics of different curves, there are two types of curves that can be used as solutions for pressure-relief curves. One is uniform motion with flexible impact characteristics, the other is sinusoidal motion without impact. Using the above two types of flexible motion rules to derive the mathematical model of the relationship between the pressure of the working cylinder, the pressure-relief time and the displacement change of the variable pump, a reasonable pressure-relief curve is obtained to achieve a smooth pressure relief.

The main factors causing pressure-relief impact are the irregular release of energy and the irregular change of flow. According to the above two kinds of flexible motion rules, the working cylinder pressure curves of energy and flow under uniform rules and sinusoidal rules are deduced, respectively, and finally, the given eccentric magnitude curve of the variable pump is obtained [28].

3.1.1. Working Cylinder Pressure-Relief According to the Energy Rule

From the energy point of view, the pressure-relief process is the release process of the working cylinder oil-compression energy and the frame elastic-deformation energy, which needs to consider what kind of relief rule can make the system smoothly reduce from high pressure to low pressure.

Because the pressure-relief process is so short, it is considered that the temperature is constant, the gas content in the oil is unchanged, and no cavitation occurs.

The initial relief pressure of the working cylinder is P_0, then its initial energy storage W_0 is,

$$W_0 = \frac{1}{2}\frac{V_0}{E}P_0^2 + \lambda P_0^2. \tag{16}$$

The mathematical model of the pressure-relief characteristic curve according to the energy uniform rule is,

$$W = W_0\left(1 - \frac{t}{T}\right) \ T \in (0, t) \tag{17}$$

where t is the pressure-relief time and T is the pressure-relief cycle.

According to Equations (13) and (17),

$$W = W_0\left(1 - \frac{t}{T}\right) = \frac{1}{2}\frac{V_0}{E}P^2 + \lambda P^2. \tag{18}$$

Therefore, the working cylinder pressure varies according to the energy uniform rule,

$$P = \sqrt{\frac{W_0\left(1 - \frac{t}{T}\right)}{\frac{1}{2}\frac{V_0}{E} + \lambda}} = P_0\sqrt{\left(1 - \frac{t}{T}\right)}. \tag{19}$$

The derivative of the working cylinder pressure is,

$$\frac{dP}{dt} = -\frac{P_0}{\sqrt{\left(1 - \frac{t}{T}\right)}}. \tag{20}$$

The mathematical model of the pressure-relief characteristic curve according to the energy sinusoidal energy rule is,

$$W = W_0\cos\frac{\pi}{2T}t \quad T \in (0, t). \tag{21}$$

According to Equations (13) and (21),

$$W = W_0\cos\frac{\pi}{2T}t = \frac{1}{2}\frac{V_0}{E}P^2 + \lambda P^2. \tag{22}$$

Therefore, the working cylinder pressure varies according to the energy sinusoidal energy rule,

$$P = \sqrt{\frac{W_0\cos\frac{\pi}{2T}t}{\frac{1}{2}\frac{V_0}{E} + \lambda}} = P_0\sqrt{\cos\frac{\pi}{2T}t}. \tag{23}$$

The derivative of the working cylinder pressure is,

$$\frac{dP}{dt} = -\frac{P_0}{2}\frac{\frac{\pi}{2T}\sin\frac{\pi}{2T}t}{\sqrt{\cos\frac{\pi}{2T}t}}. \tag{24}$$

3.1.2. Working Cylinder Pressure Relief According to the Flow Rule

The working cylinder pressure-relief process from the flow variation rule mainly considers the impact of the oil-inertia force on the sudden changes in the working cylinder flow.

The mathematical model of the pressure-relief characteristic curve according to the flow uniform rule is,

$$Q = \frac{Q_1}{t_1}t \quad t_1 \in (0, t) \tag{25}$$

where Q_1 is the system flow when the displacement of the variable pump is changed to the maximum and t_1 is the opening time when the displacement of the variable pump is changed to the maximum.

From 0 to t_1, the working cylinder oil volume variation is,

$$\Delta V = \int_0^t Qdt = \int_0^t \frac{Q_1}{t_1}tdt = \frac{1}{2}\frac{Q_1}{t_1}t^2. \tag{26}$$

The definition of effective fluid bulk modulus is,

$$E = -\frac{P - P_0}{\Delta V}V_0. \tag{27}$$

According to Equations (26) and (27),

$$\Delta V = \frac{1}{2}\frac{Q_1}{t_1}t^2 = -\frac{P - P_0}{E}V_0. \tag{28}$$

When $t = t_1$, the above equation becomes,

$$\Delta V = \frac{1}{2}Q_1 t_1 = -\frac{P_1 - P_0}{E}V_0. \tag{29}$$

where P_1 is the system pressure when the variable-pump displacement is changed to the maximum.

The flow equation of the variable-pump outlet is,

$$Q_1 = K_{qp}e_{\max} - C_p P_1 \tag{30}$$

where $e_{\max}$ is the maximum variable-pump eccentric magnitude.

According to Equations (29) and (30),

$$\frac{1}{2}\left(K_{qp}e_{\max} - C_p P_1\right)t_1 = -\frac{P_1 - P_0}{E}V_0. \tag{31}$$

Therefore, when $t = t_1$, the working cylinder pressure is,

$$P_1 = \frac{2P_0 V_0 - EK_{qp}e_{\max}t_1}{2V_0 - Et_1 C_p}. \tag{32}$$

According to Equations (30) and (32), when $t = t_1$, the working cylinder flow is,

$$Q_1 = K_{qp}e_{\max} - C_p\frac{2P_0 V_0 - EK_{qp}e_{\max}t_1}{2V_0 - Et_1 C_p}. \tag{33}$$

By the Equations (28) and (33), the working cylinder pressure varies according to the flow uniform rule,

$$P = P_0 - \frac{t^2 E}{2t_1 V_0}\left(K_{qp}e_{\max} - C_p\frac{2P_0 V_0 - EK_{qp}e_{\max}t_1}{2V_0 - Et_1 C_p}\right). \tag{34}$$

The derivative of the working cylinder pressure is,

$$\frac{dP}{dt} = -\frac{tE}{t_1 V_0}\left(K_{qp}e_{\max} - C_p\frac{2P_0 V_0 - EK_{qp}e_{\max}t_1}{2V_0 - Et_1 C_p}\right). \tag{35}$$

The mathematical model of the pressure-relief characteristic curve according to the flow sinusoidal rule is,

$$Q = \left(1 - \cos\frac{\pi}{2t_1}t\right)Q_1 \quad t_1 \in (0, t). \tag{36}$$

From 0 to t_1, the working cylinder oil volume variation is,

$$\Delta V = \int_0^t Qdt = \left(t - \frac{2t_1}{\pi}\sin\frac{\pi}{2t_1}t\right)Q_1. \tag{37}$$

According to Equations (27) and (37),

$$\Delta V = \left(t - \frac{2t_1}{\pi}\sin\frac{\pi}{2t_1}t\right)Q_1 = -\frac{P - P_0}{E}V_0. \tag{38}$$

When $t = t_1$, the above equation becomes,

$$\Delta V = \left(t_1 - \frac{2t_1}{\pi}\sin\frac{\pi}{2t_1}t_1\right)Q_1 = -\frac{P_1 - P_0}{E}V_0. \tag{39}$$

According to Equations (30) and (39),

$$\left(t_1 - \frac{2t_1}{\pi}\right)\left(K_{qp}e_{\max} - C_pP_1\right) = -\frac{P_1 - P_0}{E}V_0.$$

(40)

Therefore, when $t = t_1$, the working cylinder pressure is,

$$P_1 = \frac{\left(t_1 - \frac{2t_1}{\pi}\right)EK_{qp}e_{\max} - P_0V_0}{\left(t_1 - \frac{2t_1}{\pi}\right)EC_p - V_0}.$$

(41)

According to Equations (30) and (41), when $t = t_1$, the working cylinder flow is,

$$Q_1 = K_{qp}e_{\max} - C_p\frac{\left(t_1 - \frac{2t_1}{\pi}\right)EK_{qp}e_{\max} - P_0V_0}{\left(t_1 - \frac{2t_1}{\pi}\right)EC_p - V_0}.$$

(42)

By the Equations (38) and (42), the working cylinder pressure varies according to the flow uniform rule,

$$P = P_0 - \frac{E}{V_0}\left(t - \frac{2t_1}{\pi}\sin\frac{\pi}{2t_1}t\right)\left[K_{qp}e_{\max} - C_p\frac{\left(t_1 - \frac{2t_1}{\pi}\right)EK_{qp}e_{\max} - P_0V_0}{\left(t_1 - \frac{2t_1}{\pi}\right)EC_p - V_0}\right].$$

(43)

The derivative of the working cylinder pressure is,

$$\frac{dP}{dt} = -\frac{E}{V_0}\left(1 - \cos\frac{\pi}{2t_1}t\right)\left[K_{qp}e_{\max} - C_p\frac{\left(t_1 - \frac{2t_1}{\pi}\right)EK_{qp}e_{\max} - P_0V_0}{\left(t_1 - \frac{2t_1}{\pi}\right)EC_p - V_0}\right].$$

(44)

3.2. Variable-Pump Eccentric Magnitude Curve during the Pressure-Relief Process

The pressure-variation rule in the pressure-relief process of the OCPFHS is realized by adjusting the variable-pump eccentric magnitude. The mathematical model is used to analyze the pressure variation curve of the working cylinder during the pressure-relief process, and the control signal curve of the variable pump is obtained.

The working cylinder flow continuity equation is,

$$Q_{L1} = A_1\frac{dy}{dt} - \frac{V_0 - A_1y}{E}\frac{dP}{dt} - C_{ec1}P$$

(45)

During the pressure-relief process, the displacement of the working cylinder is zero and the flow continuity equation is,

$$Q_{L1} = -\frac{V_0}{E}\frac{dP}{dt} - C_{ec1}P.$$

(46)

The variable-pump inlet flow equation is,

$$Q = K_{qp}e - C_pP.$$

(47)

According to Equations (46) and (47),

$$Q = -\frac{V_0}{E}\frac{dP}{dt} - C_{ec1}P = K_{qp}e - C_pP.$$

(48)

Therefore, the relationship between the variable-pump eccentric magnitude and the system pressure is,

$$e = \frac{1}{K_{qp}}\left[\left(C_p - C_{ec1}\right)P - \frac{V_0}{E}\frac{dP}{dt}\right].$$

(49)

The 0.6 MN forging press system parameters under a certain condition are shown in Table 2.

Table 2. The system parameters of the 0.6 MN forging press test-bed before the pressure relief under certain condition.

Variable	Name	Value	Unit
C_p	Total leakage coefficient of variable pump	2.5×10^{-12}	$\mathrm{m^3/(Pa \cdot s)}$
C_{ec1}	External leakage coefficient of working cylinder	1.88×10^{-13}	$\mathrm{m^3/(Pa \cdot s)}$
e_{max}	Maximum eccentric magnitude of variable pump	5×10^{-3}	m
K_{qp}	Flow gain of variable pump	0.2	-
T	Pressure-relief cycle	0.6	s
P_0	Initial pressure of working cylinder	100	bar

Based on the above analysis, the working pump of the OCPFHS is simulated and the variable-pump eccentric magnitude curve under an initial pressure of 100 bar and a pressure-relief cycle at 0.6 s is obtained, as shown in Figure 4.
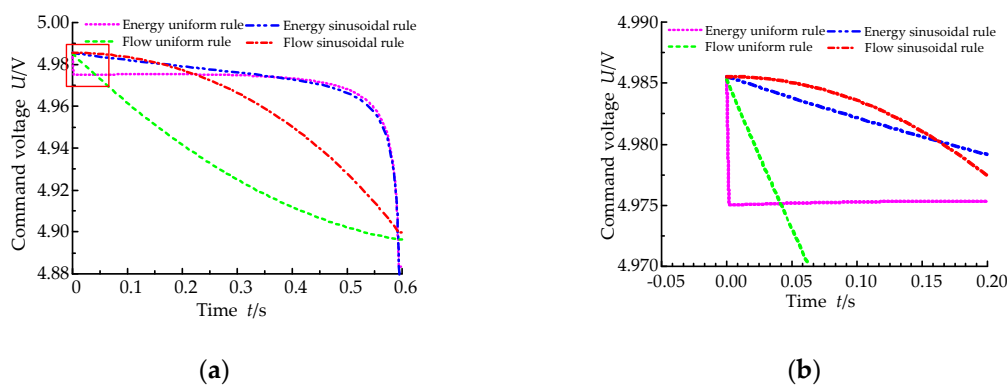

(a)

(b)

Figure 4. Simulation curves of variable-pump eccentric magnitude changes under the different pressure-relief rules. (**a**) Eccentric magnitude curve; (**b**) Partial magnification.

As shown in Figure 4, when the energy storage before pressure relief is released according to the rules, the variable-pump eccentric magnitude increases continuously. The starting point of pressure relief is not the point where the eccentric magnitude is zero (when the voltage signal is 5 V, the eccentric magnitude is zero), which is due to the existence of the variable-pump leakage, and there must be a certain dynamic balance between the flow and leakage.

When the energy uniform rule and the energy sinusoidal rule are used to relieve the pressure, the variable-pump eccentric magnitude follows the rule of initially slow and then fast, which can better suppress the pressure-relief impact. In first slow process, the variable-pump eccentric magnitude is always a smaller value, resulting in less volume increase due to oil compression and frame elastic deformation, so that the flow is smaller. When the flow uniform rule and the flow sinusoidal rule are used to relieve the pressure, the variable-pump eccentric magnitude increases from zero to the maximum, and follows the rule of initially slow and then fast.

According to the above variation rule of variable-pump eccentric magnitude in the pressure-relief process, the simulation pressure-relief curve of the working cylinder under different pressure-relief rules is obtained, as shown in Figure 5. Figure 5 shows that the pressure relief can be completed within the pressure-relief cycle when the pressure is released according to the rules. According to the energy uniform rule and energy sinusoidal rule, the pressure-relief process follows the rule of initially slow and then fast. During the initial stage of pressure relief, the pressure change is small and the time is longer, meanwhile the pressure gradient in the latter stage is increased. According to the flow uniform rule and the flow sinusoidal rule, the pressure change at the initial stage of pressure relief follows the rule of initially slow and then fast. However, in the process of pressure relief, most of the energy is relieved by a large pressure gradient, which is not conducive to suppressing the impact in the high pressure stage.
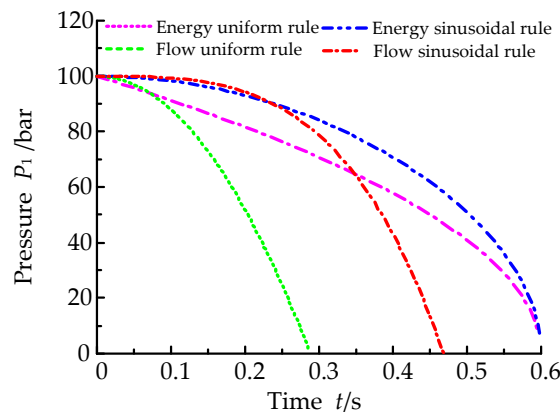
Figure 5. The simulation curve of working cylinder pressure under the different pressure-relief rules.

4. CPRC

The pressure-relief curve with a single rule can have excellent performance in a certain stage of the pressure-relief process, but it is difficult to meet the requirements of pressure-relief stability and rapidity throughout the pressure-relief process. In order to achieve the above goals, a CPRC can be used to solve the main contradiction at each stage of pressure-relief process.

Overall, in the whole cycle of the pressure-relief process, a reasonable distribution of the pressure gradient and a short pressure-relief time are fundamental to achieve pressure-relief impact control. According to the pressure-impact strength, the pressure-relief process can be divided into three stages [28]: The first stage is the high pressure stage where the pressure is about 100%–85% of the initial pressure. This stage may cause the greatest impact and requires a smaller pressure gradient. An energy sinusoidal curve can be used for pressure relief in this stage; The second stage is the medium pressure stage, the pressure is about 85%–60% of the initial pressure, and the pressure gradient can be properly increased during this stage. An energy uniform curve can be used for pressure relief in this stage; The third stage is the low pressure stage, the pressure is about 60% back pressure of the initial pressure, the impact generated during this stage is small and a large pressure gradient can be configured to shorten the pressure-relief cycle. An energy sinusoidal curve can be used in this stage.

The switching point t_a of the first and second stages is the time that the pressure drops to 85% of the initial pressure, the switching point t_b of the second and third stages is the time that the pressure drops to 60% of the initial pressure, and the end point t_c of the third stage is the time that the pressure drops to 8% of the initial pressure (taking an initial pressure of 100 bar and a back pressure of 8 bar as an example), as shown in Figure 6. At the curve-switching point, it is necessary to ensure that the two curves to be switched have the same variable-pump eccentric magnitude. Therefore, each curve needs to adopt an appropriate pressure-relief cycle.
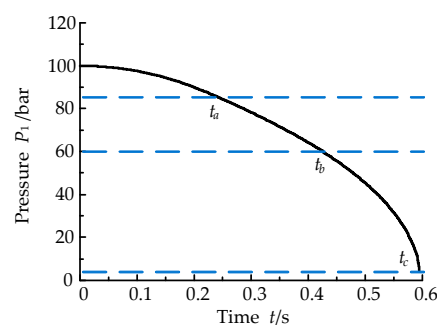

Figure 6. The switch point schematic diagram of the combined pressure-relief curve (CPRC).

The pressure-relief process is a fast transient process. The control method is based on the pressure-relief curve deduced from the pressure-relief mechanism for open-loop control. It is necessary

to calculate the switching point of the piecewise function of the combined pressure-relief curve under the particular pressure-relief cycle and initial pressure condition.

According to the energy sinusoidal curve, the pressure drops to 85% of the initial pressure at,

$$P = 0.85P_0 = P_0 \sqrt{\cos \frac{\pi}{2T_1} t_{a1}} \tag{50}$$

where t_{a1} is the time that the pressure drops to 85% of the initial pressure according to the energy sinusoidal curve and T_1 is the pressure-relief cycle of the first stage pressure-relief curve.

According to the energy sinusoidal rule and the energy uniform rule, when the pressure drops to 85% of the initial pressure, the equal eccentric magnitude value is,

$$e = \frac{1}{K_{qp}} \left[(C_p - C_{ec1})P_0 \sqrt{\cos \frac{\pi}{2T_1} t_{a1}} + \frac{V_{c1}}{E} \frac{P_0}{2} \frac{\frac{\pi}{2T_1} \sin \frac{\pi}{2T_1} t_{a1}}{\sqrt{\cos \frac{\pi}{2T_1} t_{a1}}} \right] = \frac{1}{K_{qp}} \left[(C_p - C_{ec1})P_0 \sqrt{1 - \frac{t_{a2}}{T_2}} + \frac{V_{c1}}{E} \frac{P_0}{\sqrt{1-\frac{t_{a2}}{T_2}}} \right] \tag{51}$$

where t_{a2} is the time that the pressure drops to 85% of the initial pressure according to the energy uniform curve and T_2 is the pressure-relief cycle of the second stage pressure-relief curve.

According to the energy uniform curve, the pressure drops to 85% and 60% of the initial pressure at,

$$P = 0.85P_0 = P_0 \sqrt{1 - \frac{t_{a2}}{T_2}} \text{ and} \tag{52}$$

$$P = 0.6P_0 = P_0 \sqrt{1 - \frac{t_{b1}}{T_2}} \tag{53}$$

where t_{b1} is the time that the pressure drops to 60% of the initial pressure according to the energy uniform curve.

According to the energy uniform rule and the energy sinusoidal rule, when the pressure drops to 60% of the initial pressure, the equal eccentric magnitude value is,

$$e = \frac{1}{K_{qp}} \left[(C_p - C_{ec1})P_0 \sqrt{1 - \frac{t_{b1}}{T_2}} + \frac{V_{c1}}{E} \frac{P_0}{\sqrt{1-\frac{t_{b1}}{T_2}}} \right] = \frac{1}{K_{qp}} \left[(C_p - C_{ec1})P_0 \sqrt{\cos \frac{\pi}{2T_3} t_{b2}} + \frac{V_{c1}}{E} \frac{P_0}{2} \frac{\frac{\pi}{2T_3} \sin \frac{\pi}{2T_3} t_{b2}}{\sqrt{\cos \frac{\pi}{2T_3} t_{b2}}} \right] \tag{54}$$

where t_{b2} is the time that the pressure drops to 60% of the initial pressure according to the energy uniform curve and T_3 is the pressure-relief cycle of the third stage pressure-relief curve.

According to the energy sinusoidal curve, the pressure drops to 60% of the initial pressure at,

$$P = 0.6P_0 = P_0 \sqrt{1 - \frac{t_{b2}}{T_3}} . \tag{55}$$

The OCPFHS always maintains a constant back pressure. According to the energy sinusoidal curve of the pressure-relief cycle at T_3, the pressure when it drops to the back pressure is,

$$P_b = P_0 \sqrt{\cos \frac{\pi}{2T_3} t_c} \tag{56}$$

where t_c is the time that the pressure drops to back pressure according to the energy sinusoidal curve and P_b is the back pressure.

Then, the total relief time of CPRC is,

$$t_z = t_{a1} + (t_{b1} - t_{a2}) + (t_c - t_{b2}). \tag{57}$$

In summary, the pressure equation of CPRC is,

$$P = \begin{cases} P_0 \sqrt{\cos \frac{\pi}{2T_1} t} & (0 \le t \le t_{a1}) \\ P_0 \sqrt{1 - \frac{t-(t_{a1}-t_{a2})}{T_2}} & (t_{a1} < t \le t_{a1} + (t_{b1} - t_{a2})) \\ P_0 \sqrt{\cos \frac{\pi}{2T_3} [t + t_{b2} - t_{a1} - (t_{b1} - t_{a2})]} & (t_{a1} + (t_{b1} - t_{a2}) < t \le T) \end{cases} \quad (58)$$

The variable-pump eccentric magnitude equation with CPRC is,

$$e = \begin{cases} \frac{1}{K_{qp}} \left[(C_p - C_{ec1}) P_0 \sqrt{\cos \frac{\pi}{2T_1} t} + \frac{\frac{\pi V_{c1} P_0}{2T_1} \sin \frac{\pi}{2T_1} t}{2E \sqrt{\cos \frac{\pi}{2T_1} t}} \right] & (0 \le t \le t_{a1}) \\ \frac{1}{K_{qp}} \left[(C_p - C_{ec1}) P_0 \sqrt{1 - \frac{t-(t_{a1}-t_{a2})}{T_2}} + \frac{V_{c1}}{E} \frac{P_0}{\sqrt{1 - \frac{t-(t_{a1}-t_{a2})}{T_2}}} \right] & (t_{a1} < t \le t_{a1} + (t_{b1} - t_{a2})) \\ \frac{1}{K_{qp}} \left\{ \begin{array}{c} (C_p - C_{ec1}) P_0 \sqrt{\cos \frac{\pi}{2T_3} [t + t_{b2} - t_{a1} - (t_{b1} - t_{a2})]} \\ + \frac{\frac{\pi V_{c1} P_0}{2T_3} \sin \frac{\pi}{2T_3} [t+t_{b2}-t_{a1}-(t_{b1}-t_{a2})]}{2E \sqrt{\cos \frac{\pi}{2T_3} [t+t_{b2}-t_{a1}-(t_{b1}-t_{a2})]}} \end{array} \right\} & (t_{a1} + (t_{b1} - t_{a2}) < t \le T) \end{cases} \quad (59)$$

5. Simulation Analysis

5.1. Simulation of CPRC

Through the above analysis, taking the 0.6 MN forging press experimental platform as the research object, the OCPFHS with 100 bar initial pressure and a 0.6 s pressure-relief cycle is used to simulate the corresponding variable-pump eccentric magnitude curve and the CPRC curve, as shown in Figure 7.
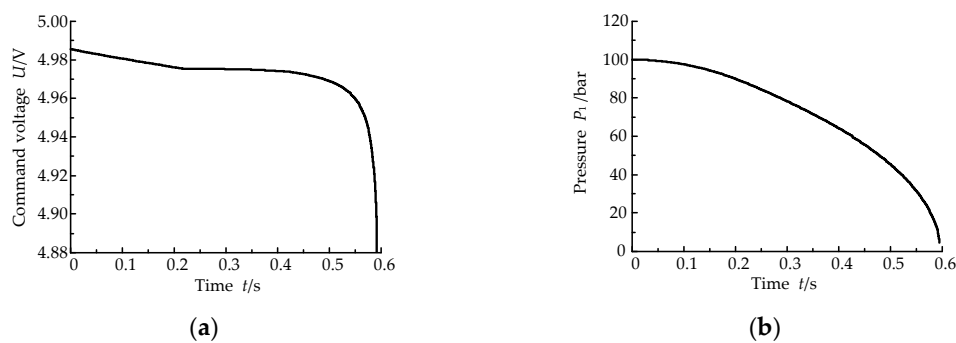

Figure 7. The simulation curve under the CPRC rule. (**a**) Eccentric magnitude curve; (**b**) Calculation CPRC.

Using the above variable-pump eccentric magnitude variation curve, the working cylinder simulation pressure-relief curve and the corresponding variable-pump eccentric magnitude curve under different pressure-relief rules are obtained, as shown in Figure 8.
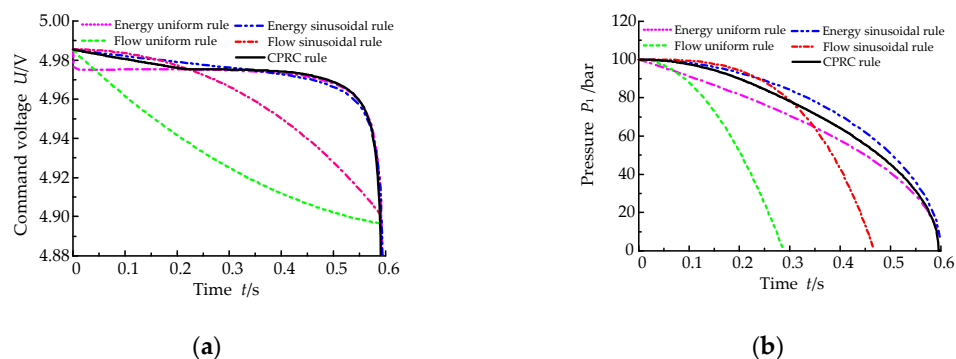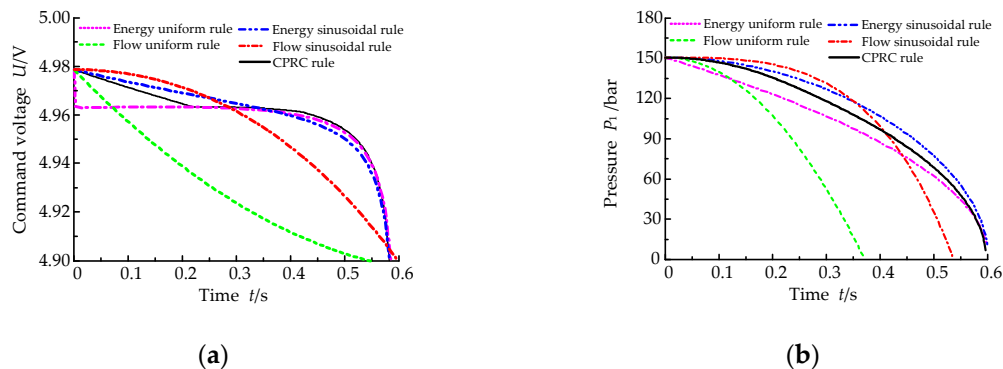

Figure 8. The simulation curve under the different pressure-relief rules under initial pressures of 100 bar. (**a**) Eccentric magnitude curves; (**b**) Calculation of CPRC.

As shown in Figure 8, the CPRC meets the requirements of pressure-relief stability and rapidity in the pressure-relief process. Compared with the single pressure-relief curve, the partial characteristics are optimized, and the advantages of different curves are taken into account.

5.2. Pressure-Relief Impact Control

Under the above pressure-relief rules, the initial pressure of 150 bar was used as the research condition to generate the working cylinder simulation pressure-relief curve and the corresponding variable-pump eccentric magnitude curve under different pressure-relief rules, as shown in Figure 9.

Figure 9. The simulation curve under the different pressure-relief rules under initial pressures of 150 bar. (**a**) Eccentric magnitude curve; (**b**) Pressure-relief curves.

Figures 8 and 9 show that in the pressure-relief initial pressure, when the storage energy of the working cylinder changes in accordance with flow uniform rule, flow sinusoidal rule, energy uniform rule, CPRC rule, and energy sinusoidal rule in turn, the working cylinder pressure-relief time increases, but it is controlled in the 0.6 s pressure-relief cycle. With the same pressure-relief curve and different initial pressures, as the pressure-relief initial pressure increases, the energy stored in the working cylinder and the pipeline increases, resulting in an increased pressure-relief gradient.

Under the above pressure-relief rules, the pressure-relief characteristics of the OCPFHS were obtained under the pressure-relief initial pressure of 100 bar and 150 bar, respectively, as shown in Figure 10.
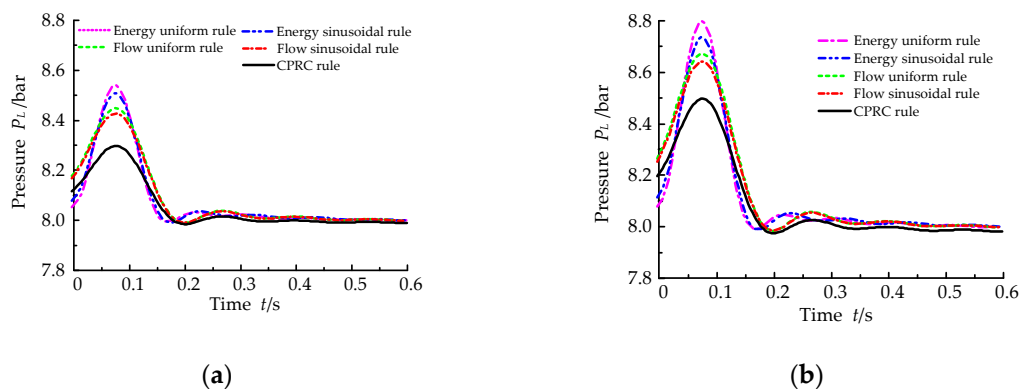

Figure 10. The pressure response curve of the pressure-relief pipe under initial pressures of 100 bar and 150 bar. (**a**) 100 bar initial pressure; (**b**) 150 bar initial pressure.

Figure 10 shows that under the same pressure-relief initial pressure, when the storage energy of the working cylinder changes in accordance with the energy uniform rule, energy sinusoidal rule, flow uniform rule, flow sinusoidal rule, and CPRC rule in turn, the pressure fluctuations of the relief pipe under the above pressure-relief rules is obviously lower than that of the step pressure-relief rule.

In addition, the pressure fluctuation peak value and frequency of the relief pipe decrease in turn and are obviously lower than other rules. With the same pressure-relief curve and different initial pressures, as the pressure-relief initial pressure increases and the pressure fluctuation in the relief pipe becomes larger.

6. Experimental Analysis

On the basis of the above theory and simulation analysis, relying on the 0.6 MN forging press experimental platform in our lab, the pressure-relief characteristics of the OCPFHS was carried out to verify the correctness of the theoretical analysis.

6.1. The 0.6 MN Forging Press Experimental Platform

The experimental platform and hydraulic system scheme of OCPFHS (Yanshan University, Qinhuangdao, China) are shown in Figures 11 and 12. The main parameters of the hydraulic system on the 0.6 MIN forging press experimental platform are shown in Table 3. The hydraulic system is mainly composed of tank, motor (Jiamusi Electric Machine Co., Ltd., jiamusi, China), MOOG's triple-link pump (MOOG China, Shanghai, China), detecting element, and low pressure charge system (Tianjin Huaman Pump Group Co., Ltd., Tianjin, China). The MOOG's triple-link pump is installed in series by two MOOG's pumps and one control oil gear pump.

An xPC-Target data acquisition and control system with 0.001 s sample time was used in the electrical control system. The MATLAB/Simulink procedure was programmed and downloaded to the xPC-Target, then the xPC-Target controlled the variable pumps by ACL6126 (D/A conversion). The pressure signals were collected by PCL1716(A/Dconversion). Interface software was developed using Labview (LabVIEW 2010, National Instruments, Austen, TX, USA, 2010) to accomplish the key parameters real-time set and display of the press.
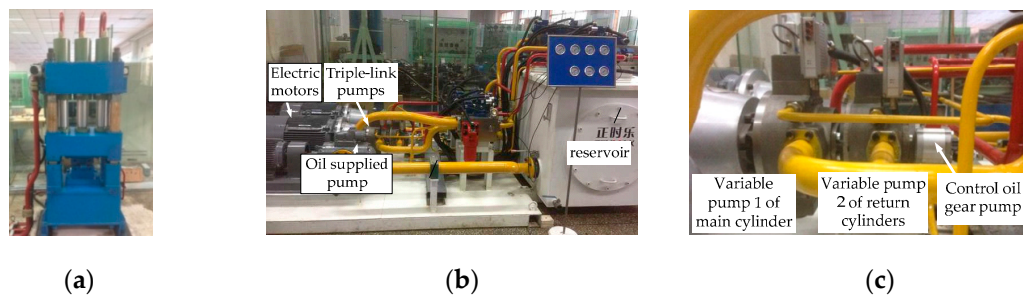

| (a) | (b) | (c) |

Figure 11. The test-bed diagram. (**a**) Hydraulic press body; (**b**) Hydraulic system of the press; (**c**) MOOG's triple-link pumps.
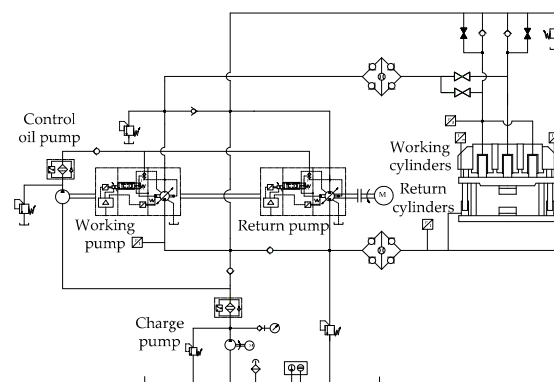

Figure 12. The test-bed hydraulic system scheme of pump-controlled system.

Table 3. The hydraulic system parameters of the 0.6MN forging press.

Name	Parameters	Note
Working cylinder diameter	0.1 m	
Return cylinder diameter	0.045 m	
Working pump displacement	80 ml/r	inherent frequency = 100Hz
Return pump displacement	45 ml/r	inherent frequency = 100Hz
Gear pump displacement	8 ml/r	
Electric motor power	30 kW	
Electric motor torque	191 N·m	
Pressure transmitter	0–40 MPa	±0.1%
Displacement sensor	700 mm	16 bit accuracy

6.2. Pressure-Relief Impact Control Analysis

A step signal was used to relieve pressure of the OCPFHS, and the experimental curves were obtained under the initial pressure of 100 bar, as shown in Figure 13. Figure 13 shows that when the OCPFHS adopts step pressure relief, the working cylinder pressure decreases rapidly, and realizes pressure relief in a short time. However, the working cylinder pressure fluctuates during the descent process, and the peak pressure in the relief pipe is 10.275 bar, which exceeds the steady pressure of 28.43%, indicating that the pressure-relief process produces a strong pressure-relief impact. In the simulation, the pressure of the charge pump in front of the working pump is given a fixed value. However, in the actual system, the charge pump had the problem of flow pulsation, so the final fluctuation phenomenon appeared. In this case, we consider the pressure to be constant. The experiment verifies the existence of pressure-relief impact under a step pressure relief. It is necessary to select a reasonable relief curve according to the system energy storage variation rule to realize the pressure-relief impact control.
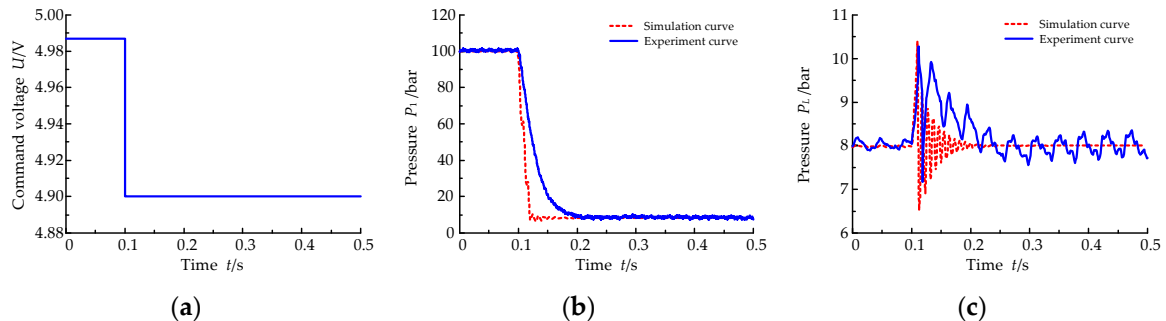

Figure 13. The experiment curves under the step pressure-relief rule. (**a**) Eccentric magnitude; (**b**) Working cylinder pressure; (**c**) Relief-pipe pressure.

The experiment on the OCPFHS was carried out by using different relief curves. The working-pump eccentric magnitude curves were shown in Figures 8 and 9, the initial pressure was 100 bar and 150 bar, respectively, and the pressure-relief cycle was 0.6 s.

Working cylinder pressure curves and relief pipe pressure curves are shown in Figures 14 and 15. As shown in Figures 14 and 15, the five pressure-relief rules above can achieve a smoother pressure relief, while the relief-pipe pressure fluctuation under the CPRC rule is smaller than that of other rules, When the initial pressure is 10 MPa and 15 MPa, the pressure impact of the pressure-relief tube decreases by 45.45% and 37.5%, respectively, which realizes the smooth pressure relief of the main cylinder. In the simulation, the pressure of the charge pump in front of the working pump is given a fixed value. However, in the actual system, the charge pump had the problem of flow pulsation, so the final fluctuation phenomenon appeared. The experimental and simulation results of the working cylinder pressure-relief process are consistent, but the pressure-relief time in the experiment was faster than that of the simulation results, mainly because the oil is in a high-speed turbulent state during the pressure-relief process. In addition, the oil movement rules are different from the states described by

the flow continuity equation. It is impossible to accurately describe the pressure-transmission rule in the pipe.
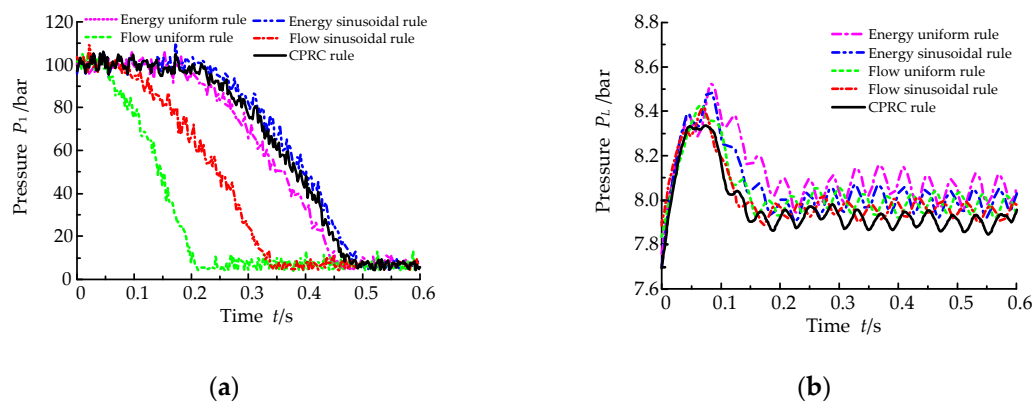

(**a**)　　　　　　　　　　　　　　　　　　　　　　(**b**)

Figure 14. The system response curve under initial pressure of 100 bar. (**a**) Working cylinder pressure; (**b**) Relief-pipe pressure.
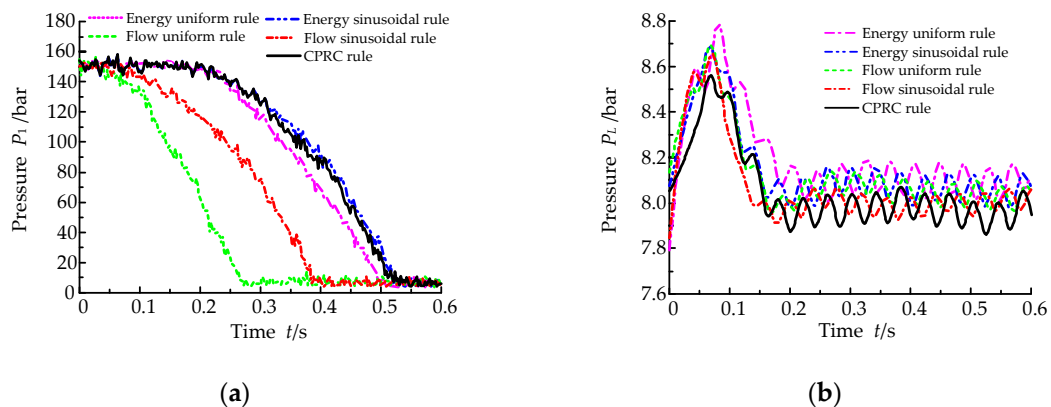

(**a**)　　　　　　　　　　　　　　　　　　　　　　(**b**)

Figure 15. The system response curve under initial pressure of 150 bar: (**a**) Working cylinder pressure; (**b**) Relief-pipe pressure.

7. Conclusions

In order to improve production efficiency of the OCPFHS, it is necessary to improve the impact characteristics of pressure relief. One of the key problems for improving the performance of forging hydraulic presses is the control method of pressure-relief impact, which comprehensively considers the period of pressure relief and impact strength. It is difficult to further improve the control performance by using the traditional method of selecting a single rule of pressure-relief curve. Therefore, it is of practical significance to study the pressure-relief curve of low impact OCPFHS. In this paper, the energy storage state of the system before pressure relief was analyzed, and the combined pressure-relief curve model was established. The control methods of quick pressure relief of the main cylinder and low impact of the pressure-relief tube were obtained. The main conclusions are as follows.

(1) In this paper, the pressure-relief impact control method on the OCPFHS was studied. When the OCPFHS adopts step pressure relief, the working cylinder pressure decreases rapidly, and realizes pressure relief in a short time. However, the working cylinder pressure fluctuates during the descent process, and the peak pressure in the relief pipe exceeds the steady pressure of 28%, indicating that the pressure-relief process produces a strong pressure-relief impact. So it is proposed that a reasonable pressure-relief curve is needed to realize the smooth pressure relief.

(2) The method of CPRC was put forward to effectively control the pressure-relief effect of the OCPFHS. The mathematical model of CPRC was established, the working pump eccentric magnitude

during the pressure-relief process was planned, and the smooth pressure relief of the working cylinder was realized.

(3) The simulation and experimental research on the pressure-relief impact control of OCPFHS were carried out. The working cylinder response characteristics and relief-pipe pressure response were analyzed under the initial pressures of 100 bar and 150 bar. The results show that in the pressure-relief initial pressure, when the storage energy of the working cylinder changes in accordance with flow uniform rule, flow sinusoidal rule, energy uniform rule, CPRC rule, and energy sinusoidal rule in turn, the working cylinder pressure-relief time increases but it is controlled in the 0.6 s pressure-relief cycle. With the same pressure-relief curve and different initial pressures, as the pressure-relief initial pressure increases, the energy stored in the working cylinder and the pipeline increases, resulting in an increased pressure-relief gradient.

References

1. Yu, H.Y.; Tang, J.L.; Hu, J. Research on Hydraulic System of Speed Forging Hydraulic Machine. *Appl. Mech. Mater.* **2012**, *192*, 123–127. [CrossRef]
2. Gao, J.; Yan, G.Y.; Peng, G.Y.; Xi, G.N. Experiment study on performances of servo pump used in hydraulic press machine. *Adv. Mater. Res.* **2012**, *516*, 892–895. [CrossRef]
3. Quan, L. Current state, problems and the innovative solution of electro-hydraulic technology of pump-controlled cylinder. *Chin. J. Mech. Eng.* **2008**, *44*, 87–92. [CrossRef]
4. Quan, L.; Xu, X.Q.; Yan, Z.; Zhang, X.J. A new kind of pilot controlled proportional direction valve with internal flow feedback. *Chin. J. Mech. Eng.* **2010**, *23*, 60–65. [CrossRef]
5. Su, W.H.; Jiang, J.H. Direct drive volume control electro-hydraulic servo ship rudder. *Key Eng. Mater.* **2010**, *439*, 1388–1392. [CrossRef]
6. Axin, M.; Eriksson, B.; Krus, P. Flow versus pressure control of pumps in mobile hydraulic systems. *Proc. Inst. Mech. Eng. Part I J. Syst. Control Eng.* **2014**, *228*, 245–256. [CrossRef]
7. Cetinkunt, S.; Pinsopon, U.; Chen, C.; Egelja, A.; Anwar, S. Positive flow control of closed-center electrohydraulic implement-by-wire systems for mobile equipment applications. *Mechatronics* **2004**, *14*, 403–420. [CrossRef]
8. Minav, T.A.; Laurila, L.; Pyrhönen, J.J. Analysis of electro-hydraulic lifting system's energy efficiency with direct electric drive pump control. *Autom. Constr.* **2013**, *30*, 144–150. [CrossRef]
9. Zimmerman, J.; Hippalgaonkar, R.; Ivantysynova, M. Optimal control for the series-parallel displacement controlled hydraulic hybrid excavator. In Proceedings of the ASME 2011 Dynamic Systems and Control Conference and Bath/ASME Symposium on Fluid Power and Motion Control, Arlington, VA, USA, 31 October–2 November 2011; pp. 129–136.
10. Zhao, H.; Zhang, H.J.; Quan, L.; Li, B. Characteristics of asymmetrical pump controlled differential cylinder speed servo system. *Chin. J. Mech. Eng.* **2013**, *49*, 170–176. [CrossRef]
11. Song, Y.; Kong, X.D.; Yao, J.; Wang, Z. Oil hydraulic press control characteristics with open variable pump-controlled system. *China Mech. Eng.* **2016**, *27*, 1031–1038.
12. Yao, J.; Ren, X.H.; Cao, X.M.; Zhao, J.S.; Kong, X.D. Experimental study on energy consumption characteristics of fast hydraulic forging press with open variable pump-controlled system. *China Mech. Eng.* **2017**, *28*, 462–470.
13. Yao, J.; Wang, P.; Cao, X.M.; Wang, Z. Independent volume-in and volume-out control of open circuit pump-controlled asymmetric cylinder system. *J. Zhejiang Univ. Sci. A* **2018**, *19*, 203–210. [CrossRef]

14. Yao, J.; Wang, P.; Dong, Z.S.; Kong, X.D. Coupling characteristics of independent volume-in and volume-out control for open circuit pump-controlled asymmetric cylinder systems. *China Mech. Eng.* **2017**, *28*, 1639–1645.

15. Ai, C.; Kong, X.D.; Liu, S.K.; Song, Y.; Chen, G. Study on the influence factors of control characteristics of accumulator fast forging circuit for pump-controlled hydraulic press. *Forg. Stamping Technol.* **2014**, *39*, 89–95.

16. Ai, C.; Liu, Y.J.; Song, Y.; Kong, X.D. Research on flow pressure compound position control of open circuit hydraulic pump-controlled forging press system. *China Mech. Eng.* **2016**, *27*, 1705–1715.

17. Prihatin, J.Y.; Kustanto, H.; Pambudi, S.; Nagoro, I.H.A. Study of fluids pressure in hydraulic press machine using L8 orthogonal array. *AIP Conf. Proc.* **2018**, *1*, 020005.

18. Yao, J.; Kong, X.D. Study on process control characteristics of 22MN fast forging hydraulic press. *Adv. Mater. Res.* **2011**, *201*, 2258–2262. [CrossRef]

19. Han, H.Y.; Li, H.Z.; Li, J.; Miao, K.; Wang, J.; Wei, C. Analyzing Nonlinear system stability of a new hydraulic bilateral rolling shear. *ISIJ Int.* **2016**, *56*, 1789–1795. [CrossRef]

20. Henclik, S. Analytical solution and numerical study on water hammer in a pipeline closed with an elastically attached valve. *J. Sound. Vib.* **2018**, *417*, 245–259. [CrossRef]

21. Ding, H.; Zhao, J. Dynamic characteristic analysis of replenishing/leaking parallel valve control systems. *Automatika* **2017**, *58*, 182–194. [CrossRef]

22. Wang, C.B.; Quan, L.; Ou, H. The method of restraining hydraulic impact with active adjusting variable damping. *Proc. Inst. Mech. Eng. Part C* **2019**, *233*, 3785–3794. [CrossRef]

23. Yao, J.; Li, B.; Kong, X.D.; Zhou, F. Displacement and dual-pressure compound control for fast forging hydraulic system. *J. Mech. Sci. Technol.* **2016**, *30*, 353–363. [CrossRef]

24. Zhang, L.; Xu, H.; Pan, C.; Zhang, X.; Zou, T. Analysis of unrestrained curve of rectangular piston ring based on energy principle. In Proceedings of the 2014 13th International Conference on Control Automation Robotics & Vision (ICARCV), Singapore, 10–12 December 2014; pp. 1695–1699.

25. Fu, L.; Wei, J.; Qiu, M. Dynamic characteristics of large flow rating electro-hydraulic proportional cartridge valve. *Chin. J. Mech. Eng.* **2008**, *21*, 57–62. [CrossRef]

26. Pan, C. Cavity Pressure Relief Process Analysis and Design of a New Relief Valve. Master's Thesis, Taiyuan University of Technology, Taiyuan, China, 2012.

27. Zhao, Y. The Modeling and Simulation Study on Cam-Tape Axial Piston Proportional Pump and Hydraulic Hosepipe. Master's Thesis, Taiyuan University of Technology, Taiyuan, China, 2005.

28. Shen, W.Q. The Pressure Discharge Impact and Its Reduction Technology Research of Large Press. Master's Thesis, Central South University, Changsha, China, 2013.